Supporting Information

Simple-to-Apply Wetting Model to Predict Thermodynamically Stable and Metastable Contact Angles on Textured/Rough/Patterned Surfaces

Yair Kaufman[a,b,j,*], Szu-Ying Chen[a,j], Himanshu Mishra[a,c], Alex M. Schrader[a], Dong Woog Lee[d], Saurabh Das[a], Stephen H. Donaldson, Jr.[a,e], and Jacob N. Israelachvili[a,f]

[a] Department of Chemical Engineering, University of California at Santa Barbara, CA 93106, USA.

[b] Zuckerberg Institute for Water Research, The Jacob Blaustein Institutes for Desert Research, Ben-Gurion University of the Negev, Sede Boqer Campus 84990, Midreshet Ben-Gurion, Israel.

[c] Now at the Water Desalination and Reuse Center, Biological and Environmental Science and Engineering Division, King Abdullah University of Science and Technology, Thuwal 23955-6900, Saudi Arabia.

[d] School of Energy and Chemical Engineering, Ulsan National Institute of Science and Technology (UNIST), UNIST-gil 50, Ulsan 689-798, Republic of Korea.

[e] Now at the Département de Physique, Ecole Normale Supérieure, PSL Research University, CNRS, 24 rue Lhomond
75005 Paris, France.

[j] Authors who contributed equally to this work.

[f] Materials Department, University of California at Santa Barbara, CA 93106, USA.

[*] To whom correspondence should be addressed. yairkau@bgu.ac.il.

Simple-to-Apply Wetting Model to Predict Thermodynamically Stable and Metastable Contact Angles on Textured/Rough/Patterned Surfaces

1. The droplet Laplace pressure and droplet hydrostatic pressure (i.e., gravity) have negligible effect on the area of the liquid-vapor interface within a single cavity

As shown in Fig. S1, to balance the droplet Laplace pressure, the curvature of the liquid-vapor interface within the cavity should equal the curvature of the macroscopic droplet, $1/R$. Based on simple geometry analysis, the liquid-vapor interface within a cavity bulges into the cavity by:

$$h' = R\left(1 - \cos\left(\operatorname{asin}\frac{r}{R}\right)\right), \tag{S1}$$

where r is the radius of the cavity opening.

The areas of the flat liquid-vapor interface, A_{f}, and the area of the curved liquid-vapor interface, assuming a spherical cap, is given by:

$$A_{\mathrm{f}} = \pi r^2, \tag{S2}$$

$$A_{\mathrm{cap}} = \pi(r^2 + h'^2), \tag{S3}$$

Therefore, the change in area as the liquid-vapor within a single cavity, which is expressed in fraction of a flat liquid-vapor area, is given by:

$$\Delta A = \frac{A_{\mathrm{cap}} - A_{\mathrm{f}}}{A_{\mathrm{f}}} = \frac{\pi h'^2}{\pi r^2}. \tag{S4}$$

Based on Eq. S4, for a droplet of R=1000 μm, which is a typical value for the droplets we used in our experiments, $\Delta A = 2.5 \times 10^{-7}$ for r=1 μm (smallest cavity in our experiments), and $\Delta A = 2.3 \times 10^{-4}$ r=30 μm (largest cavity in our experiments). Hence, the effect of droplet Laplace pressure on the area of the liquid-vapor interface within a cavity was negligible in all our experiments.

The hydrostatic pressure, i.e., the effect of gravity, is given by $\sim 2\rho g R$, where ρ is the mass density of water. The droplet Laplace pressure is given by $\sim 2\gamma_{\mathrm{LV}}/R$. The ratio of hydrostatic to Laplace pressure is $\frac{\rho g R^2}{\gamma_{\mathrm{LV}}} \cong 0.1$; hence, the effect of gravity is smaller than the effect of

Laplace pressure. Therefore, both hydrostatic pressure and the droplet Laplace pressure were negligible in all our experiments.

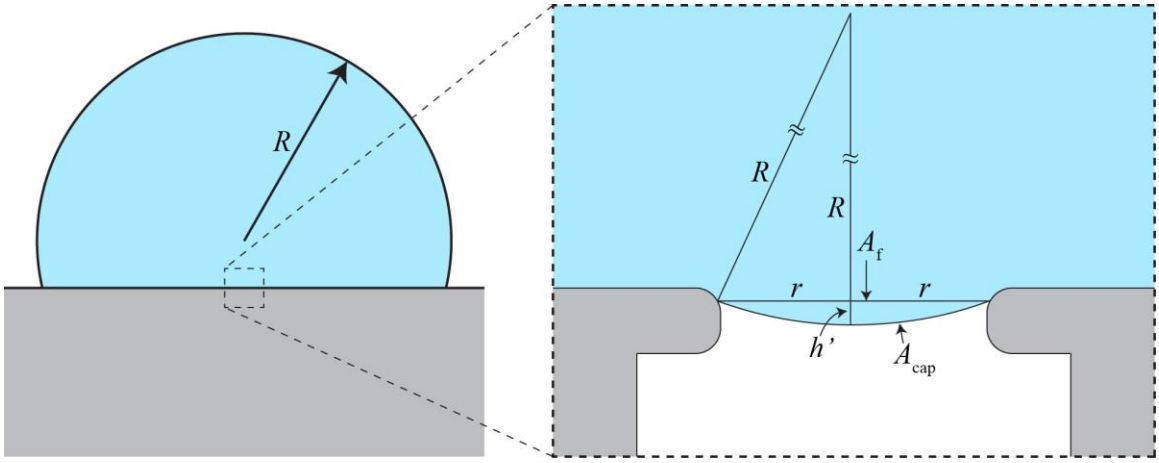

Figure S1: Estimating the effect of droplet Laplace pressure and gravity on the area of the liquid-vapor interface within a cavity.

2. Derivation of $\left(\frac{dA_C}{dA_P}\right)_{V_0} = cos\beta$

For this derivation, let us define A_C, A_f as the curved and the flat areas of the truncated droplet and V_0 is the droplet volume (see Fig. 2 in the main text). Based on geometry:

$$A_C = 2\pi R^2(1-\cos\theta_0), \tag{S5}$$
$$A_P = \pi R^2 sin^2\theta_0$$
$$V_0 = \frac{\pi R^3}{3}\,(1-\cos\theta_0)(2+\cos\theta_0)$$

Now,

$$\frac{dA_C}{d\theta_0} = 2\pi\left[2R(1-\cos\theta_0)\,\frac{dR}{d\theta_0} + R^2(\sin\theta_0)\right] \tag{S6}$$

$$\frac{dA_P}{d\theta_0} = \pi\left[2R\sin^2\theta_0\,\frac{dR}{d\theta_0} + 2R^2\sin\theta_0\cos\theta_0\right]$$

For fixed volume:

$$\frac{dV_0}{d\theta_0} = 0 \implies \frac{\pi}{3}\,\frac{d}{d\theta_0}\left(R^3(1-\cos\theta_0)^2(2+\cos\theta_0)\right) = 0 \implies \tag{S7}$$

$$\frac{dR}{d\theta_0} = \frac{-R\sin\theta_0\,(1+\cos\theta_0)}{(1-\cos\theta_0)(2+\cos\theta_0)}$$

By inserting Eq. S7 into S6 we get:

$$\frac{dA_C}{d\theta_0} = \frac{-2\pi R^2\sin\theta_0\cos\theta_0}{2+\cos\theta_0} \tag{S8}$$

$$\frac{dA_P}{d\theta_0} = -2\pi R^2\sin\theta_0\left(\frac{1}{2+\cos\theta_0}\right).$$

Therefore

$$\frac{dA_C}{d\theta_0}\,\frac{d\theta_0}{dA_P} = \frac{dA_c}{dA_P} = \cos\theta_0. \tag{S9}$$

3. Derivation of the 'wetting equation' employing an energy minimization approach

The same approach that was used to derive the Young equation, Eq. 8, was used to derived the 'wetting equation, that can be used for calculating the contact angles on textured (rough) surfaces. The 'wetting equation' should be generally applicable to any surface topology, as long as the size of the drop is significantly larger than the dimensions of the cavities (otherwise the assumption of constant V_0 breaks down as the liquid penetrates into the cavities).

For deriving the 'wetting equation', we consider now the case of a droplet of Phase 1 coming into contact with a *textured* (rough) solid surface S in the presence of Phase 2 (see Fig. 2B. For the case of non-flat geometry, we consider separately the state of the cavities – either fully-filled or partially-filled or empty of Phase 1, or vice versa of Phase 2 – *underneath* versus *outside* of the spreading droplet (see Fig. 2B Steps II and III), with the contributions from the latter denoted by the superscript 'O'. Proceeding in the same way as with the derivation of the Young equation, we write the total interacial energy of the drop at the thermodynamic minima as

$$E_0 = \gamma_{12}\left(A_{\mathrm{C}} - A_{\mathrm{C},0}\right) + \gamma_{12}\left(A_{12} - A_{12}^{\mathrm{O}}\right) + (\gamma_{1\mathrm{S}} - \gamma_{2\mathrm{S}})\left[\left(A_{1\mathrm{S}} - A_{1\mathrm{S}}^{\mathrm{O}}\right)\right], \tag{S10}$$

where A_{XY} is the real area of contact between Phase X and Phase Y (see Fig. 2B) for X and Y being either Phase 1, Phase 2, or S; and the superscript 'O' refers to the cavities outside of the wetting droplet.

Normalizing the areas of contact by the projected area, A_{P}, we get

$$E_0 = \gamma_{12}\left(A_{\mathrm{C}} - A_{\mathrm{C},0}\right) + \gamma_{12}\left[\left(A_{\mathrm{P}}\phi_{12} - A_{\mathrm{P}}\phi_{12}^{\mathrm{O}}\right)\right] + (\gamma_{1\mathrm{S}} - \gamma_{2\mathrm{S}})\left[\left(A_{\mathrm{P}}\phi_{1\mathrm{S}} - A_{\mathrm{P}}\phi_{1\mathrm{S}}^{\mathrm{O}}\right)\right], \tag{S11}$$

where ϕ_{XY} is the ratio of A_{XY} to A_{P} (see Fig. 2B).

In the subsequent step, if an infinitesimally small perturbation is made from the equilibrium configuration, which involves an increase or decrease in Phase 1-Phase 2 and Phase 1-Solid interfaces by $\mathrm{d}A_{\mathrm{C}}$ and $\mathrm{d}A_{\mathrm{P}}$, the surface energy changes to

$$\begin{aligned} E_0 + \mathrm{d}E = {} & \gamma_{12}\left(A_{\mathrm{C}} + \mathrm{d}A_{\mathrm{C}} - A_{\mathrm{C},0}\right) + \gamma_{12}(A_{\mathrm{P}} + \mathrm{d}A_{\mathrm{P}})\left[\left(\phi_{12} - \phi_{12}^{\mathrm{O}}\right)\right] \\ & + (\gamma_{1\mathrm{S}} - \gamma_{2\mathrm{S}})(A_{\mathrm{P}} + \mathrm{d}A_{\mathrm{P}})\left[\left(\phi_{1\mathrm{S}} - \phi_{1\mathrm{S}}^{\mathrm{O}}\right)\right], \end{aligned} \tag{S12}$$

The contact angle changes to $\theta_t + d\theta$, and the difference in surface energies is given by

$$dE = \gamma_{12}\left[dA_C + dA_P\left(\phi_{12} - \phi_{12}^O\right)\right] + (\gamma_{1S} - \gamma_{2S})\left[\left(\phi_{1S} - \phi_{1S}^O\right)\right]dA_P, \quad \text{(S13)}$$

Since the liquid drop was at thermodynamic equilibrium, the derivative of surface energy should be zero:

$$\left(\frac{dE}{dA_P}\right)_{V_0} = \gamma_{12}\left[\frac{dA_C}{dA_P} + \left(\phi_{12} - \phi_{12}^O\right)\right] + (\gamma_{1S} - \gamma_{2S})\left[\left(\phi_{1S} - \phi_{1S}^O\right)\right] = 0. \quad \text{(S14)}$$

Next, we employ the geometric relationship given in Eq. 7 (in the main text) and obtain

$$\gamma_{12}\left[\cos(\theta_t + d\theta) + \left(\phi_{12} - \phi_{12}^O\right)\right] + (\gamma_{1S} - \gamma_{2S})\left[\left(\phi_{1S} - \phi_{1S}^O\right)\right] = 0, \quad \text{(S15)}$$

which yields a 'wetting equation' for calculating macroscopic contact angles (θ_t):

$$\cos\theta_t = \cos\theta_0\left(\phi_{1S} - \phi_{1S}^O\right) - \left(\phi_{12} - \phi_{12}^O\right). \quad \text{(S16)}$$

4. Condensation of liquid in the cavities outside the droplet

The interfacial energy of an empty cavity outside the droplet, $E^{\mathrm{O}}_{\mathrm{empty}}$ (the superscript 'O' stands for outside of the cavity) is given by (see Fig. S4B):

$$E^{\mathrm{O}}_{\mathrm{empty}} = A_{\mathrm{LS(max)}}\gamma_{\mathrm{SV}}, \tag{S17}$$

where $A_{\mathrm{LS(max)}}$ is the entire Solid-Vapor contact area for a repeating unit (in this case it is a single cavity). Note that for the sake of consistency, we used the subscript 'LS(max)', which is the maximum Liquid-Solid contact area in the case where the cavity is 'fully-filled' (i.e., there is no liquid-vapor interface anywhere within the cavity).

The interfacial energy of a partially-filled cavity, $E^{\mathrm{O}}_{\mathrm{filled}}$, is given by (see Figs S4C and S4D)

$$E^{\mathrm{O}}_{\mathrm{filled}} = A^{\mathrm{O}}_{\mathrm{LS}}\gamma_{\mathrm{SL}} + A^{\mathrm{O}}_{\mathrm{LV}}\gamma_{\mathrm{LV}} + A^{\mathrm{O}}_{\mathrm{SV}}\gamma_{\mathrm{SV}}, \tag{S18}$$

where $A^{\mathrm{O}}_{\mathrm{LS}}$, $A^{\mathrm{O}}_{\mathrm{LV}}$ and $A^{\mathrm{O}}_{\mathrm{SV}}$ are the Solid-Liquid, Liquid-Vapor and Solid-Vapor contact areas outside the droplet, respectively.

Considering that $\gamma_{\mathrm{LS}} + \gamma_{\mathrm{LV}}\cos\theta_0 = \gamma_{\mathrm{SV}}$ (Young equation) and $A^{\mathrm{O}}_{\mathrm{LS}} + A^{\mathrm{O}}_{\mathrm{SV}} = A_{\mathrm{LS(max)}}$ (see Figs. S1B, C and D), the change in energy is:

$$\Delta E^{\mathrm{O}} = E^{\mathrm{O}}_{\mathrm{filled}} - E^{\mathrm{O}}_{\mathrm{empty}} = A^{\mathrm{O}}_{\mathrm{LV}}\gamma_{\mathrm{LV}} - A^{\mathrm{O}}_{\mathrm{LS}}\gamma_{\mathrm{LV}}\cos\theta_0 \tag{S19}$$

Eq. S19 shows that if $\theta_0 > 90°$ (i.e., $\cos\theta_0 < 0$) then $\Delta E^{\mathrm{O}} > 0$, hence condensation in the cavities outside of the droplet is not thermodynamically favorable for any type (shape) of cavities. On the other hand, when $\theta_0 < 90°$ condensation in the cavities that are outside of the droplet is thermodynamically favorable ($\Delta E^{0} < 0$) when $\cos\theta_0 > A^{\mathrm{O}}_{\mathrm{LV}}/A^{\mathrm{O}}_{\mathrm{SL}}$.

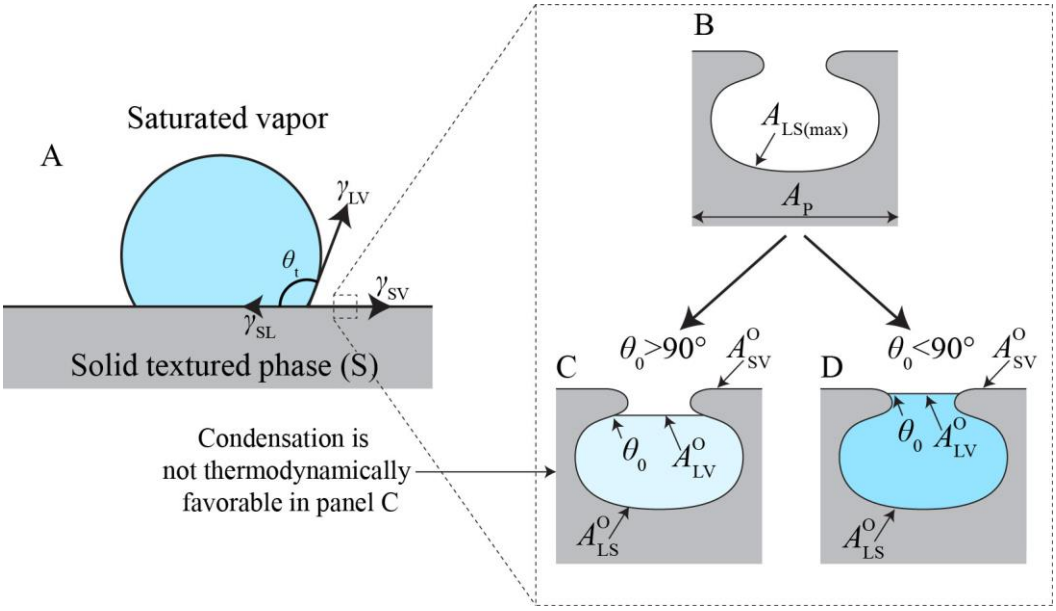

Figure S4: When the vapor around the droplet is saturated, which is often the case in close vicinity to a droplet, cavities outside of the droplet can get filled by condensation (Panel A and B). Eq. S19 shows that when $\theta_0 > 90°$ (Panel C) then cavities of any shape that are outside the droplet are empty at thermodynamic equilibrium; whereas these cavities can get filled by condensation when $\theta_0 < 90°$ and $\cos\theta_0 > A^O_{LV}/A^O_{LS}$, as illustrated in panel D.

5. Derivation of the total energy of a droplet on textured surface

Considering the Young equation and the 'wetting equation' for the 'partially-filled | empty' wetting state, Eq. 12, the change in the total interfacial energy of a droplet on a texture surface is given by:

$$\Delta E_{\text{total}} = \gamma_{\text{LV}}(A_{\text{C}} - A_{\text{P}} \cos\theta_{\text{t}}) - \gamma_{\text{LV}} A_{\text{C},0}. \quad \text{(S20)}$$

Assuming the droplet forms a truncated sphere on the textured surface, thus $A_{\text{C}} = 2\pi R^2(1 - \cos\theta_{\text{t}})$, $A_{\text{P}} = \pi R^2 \sin^2\theta_{\text{t}}$, and $R = 4^{1/3} R_0 (2 - 3\cos\theta_{\text{t}} + \cos^3\theta_{\text{t}})^{-1/3}$,[1], Eq. S20 can be rewritten:

$$E_{\text{total}} = E_{\text{fin}} - E_{\text{init}} = \frac{4\pi R_0^3 \gamma_{\text{LV}}}{4^{1/3}(2-3\cos\theta_{\text{t}}+\cos^3\theta_{\text{t}})^{-1/3}} - 4\pi R_0^2 \gamma_{\text{LV}}, \quad \text{(S21)}$$

which is Eq. 24 in the main text.

6. Experimental Demonstration: Preparation and Characterization of the Samples

6.1 Preparation of the re-entrant cavities

The fabricated of the re-entrant cavities is depicted in Fig. S2. One-sided silicon wafer with 1.4 μm top layer of thermally-grown silica layer (University Wafers) was used as a starting point. Using standard lithography procedures, arrays of cylinders were vertically etched through the silica layer using ICP (Panasonic E626I). Next, the re-entrant cavities were done by isotropically etching silicon under the silica layer using XeF2 (Xetch). Lastly, Deep RIE (PlasmaTherm) was employed to vertically etch the silicon cavities.

A silicon wafer with a top layer of 10 μm thermally grown silica (University Wafers) was used as a substrate for the fabrication of the cavities without the re-entrant (Fig. 8B and E). Then, using standard lithography procedures, arrays of cylinders were vertically etched through the silica layer using ICP (Panasonic E626I).

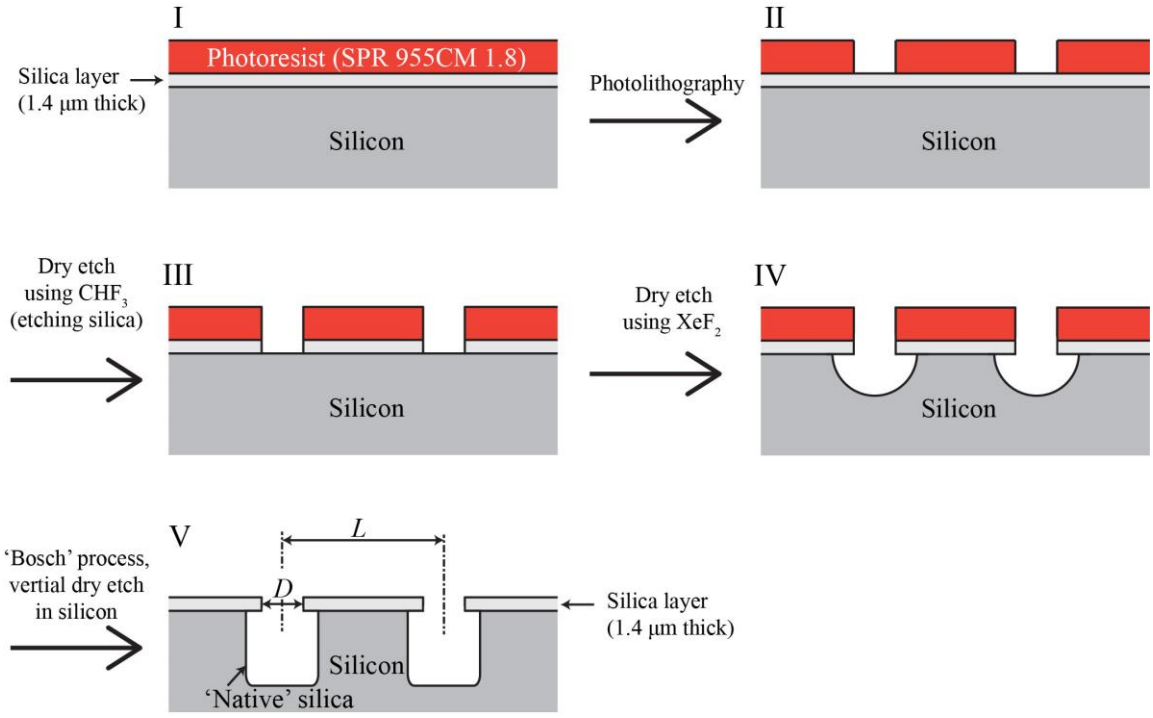

Figure S6.1: Fabrication process of the re-entrant cavities. The pristine substrate, shown in Panel I, was a silicon wafer with a 1.4 μm thick thermally-grown silica. Panel II shows the first step of the process, where a layer of photoresist is spin-coated over the substrate, followed by exposing the photoresist to a UV light (the common lithography procedure) through a mask in order to create an array of "openings" in the photoresist. Panel III shows the ICP dry etch step, using CHF_3, in order to vertically etch the silica. Next, in Panel IV, XeF_2 was used to isotropically etch the silicon in order to create the re-entrant cavities. In the last step, illustrated in Panel V, the 'Bosch' process was used to deepen the cavities.

6.2 Preparation of the Non Re-entrant Cavities

One-sided silicon wafers with 10 μm thermally-grown silica layer (University Wafers) were used as a starting point. Using standard lithography procedures, arrays of ~8 μm deep cylinders were vertically etched through the silica layer using ICP (Panasonic E626I).

6.3 Contact angle measurements

Using OCA-15 Pro (Dataphysics), a 1 μl droplet of deionized water (18.2 MΩ cm, Milli-Q) was deposited on the samples. Then, the droplet was allowed to equilibrate for 30 s. Using a commercially available software (Dataphysics), the droplet on the sample was modeled as a truncated sphere. The reported contact angles, θ_t, were the angles between the tangent (at the liquid-vapor-solid triple line) to the truncated sphere and the base of the sphere (see Fig. 7B).

6.4 Fluorescence imaging

Two-photon fluorescence microscopy (Olympus Fluoview 1000MPE) images were captured using water immersion objective lens. Fluorescein isothiocyanate (FITC) at 0.1 mg/mL was used in deionized water. Measurements were made at ~23°C. A 800 nm IR laser was used for excitation, and emission was observed at 530 nm.

6.5 Contact angle measurements using canola oil on textures with and without re-entrant cavities

This section is an experimental demonstration of the 'wetting model' using canola (γ_{LV}~35 mN/m)[2], which represents a liquid with low surface tension (the interfacial energy of canola oil/air) . More details can be found in Section "Experimental Demonstration of the 'wetting model'" in the manuscript.

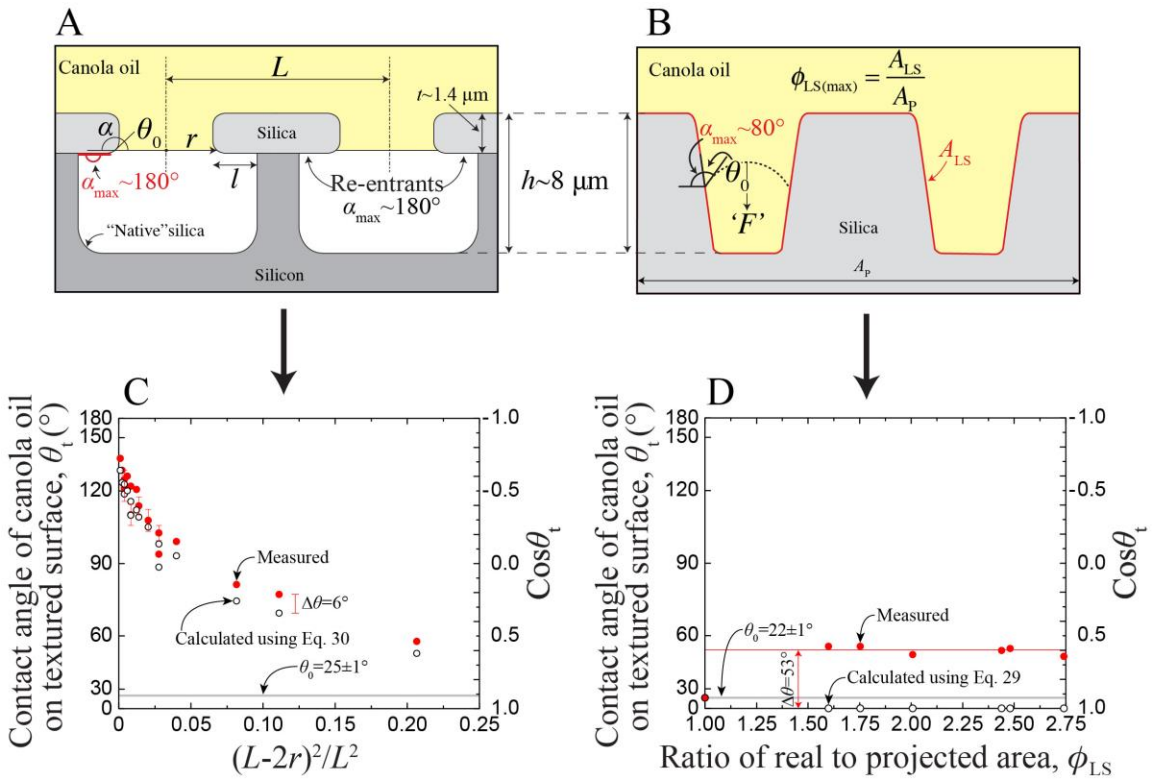

Figure S6.2: Experimental demonstration of the 'wetting model'. Two types of silica (intrinsic contact angle of canola oil is θ_0~25°) textures were prepared: (1) re-entrant cavities, where α_{max} ~180°, as shown in Panel, and (2) non-re-entrant cavities, where α_{max} ~80°, as shown in Panel B. The 'wetting model' predicts that when $\alpha_{max} + \theta_0 > 180°$ and $\theta_0 < 90°$, such as the case of canola oil on the re-entrant cavities, the 'partially-filled | empty' (Cassie-Baxter) wetting state is metastable. On the other hand, when $\alpha_{max} + \theta_0 < 180°$, such as in the case of canola oil on the non-re-entrant cavities, canola oil spontaneously (no energy barrier) fills the cavities and the 'fully-filled | empty' (Wenzel state) wetting state is formed. Panels C and D show the measured contact angles, θ_t, and the calculated contact angles for cavities with (Panel C, Eq. 22) and without (Panel D, Eq. 21) re-entrants.

7. Experimental Section: Evaluating the State of the Cavities Outside the Droplet

For the re-entrant cavities, the cavities outside the droplet are partially-filled if

$$\cos\theta_0 > A_{\mathrm{LV}}^0/A_{\mathrm{LS}}^0, \tag{S22}$$

Where A_{LV}^0 and A_{LS}^0 are the liquid-vapor and liquid-solid interfaces outside of the droplet. Hence, for the re-entrant cavities, equality S22 can be written as

$$\cos\theta_0 > \frac{\pi r^2}{2\pi(r+l)(h-t)+\pi(r+l)^2+\pi(r+l)^2-\pi r^2}. \tag{S23}$$

Based on Figs. 8A and D (in main text), the height of the cavity, h, is ~8 μm, the thickness of the overhanging layer, t, is ~1 μm, and the size of the re-entrant, l, is ~0.3 μm. Therefore, based on equality S23, and assuming that $l \ll r$, one can conclude that when $r < 34$ μm, which was the case of all the samples we prepared for this experimental study, equality S22 is satisfied and the 'fully-filled | partially-filled' wetting (Eq. 9) state is thermodynamically favorable wetting state.

For the cavities without re-entrants, equality S22 is satisfied when

$$\cos\theta_0 > \frac{\pi r^2}{2\pi rh+\pi r^2}. \tag{S24}$$

Thus, for cavities without re-entrants, when $r < 38$ μm, which was the case of the all the samples we prepared for this experimental study, the 'fully-filled | partially-filled' (Eq. 9) wetting state is the thermodynamically stable wetting state.

8. Summary

Fig. S8 summarizes the conditions that would yield the three different wetting states, namely: 'partially-filled | empty', 'fully-filled | empty' and 'fully-filled | partially-filled'. The figure also defines the conditions in which each wetting state is transient, metastable or thermodynamically stable (see more details in the main text).

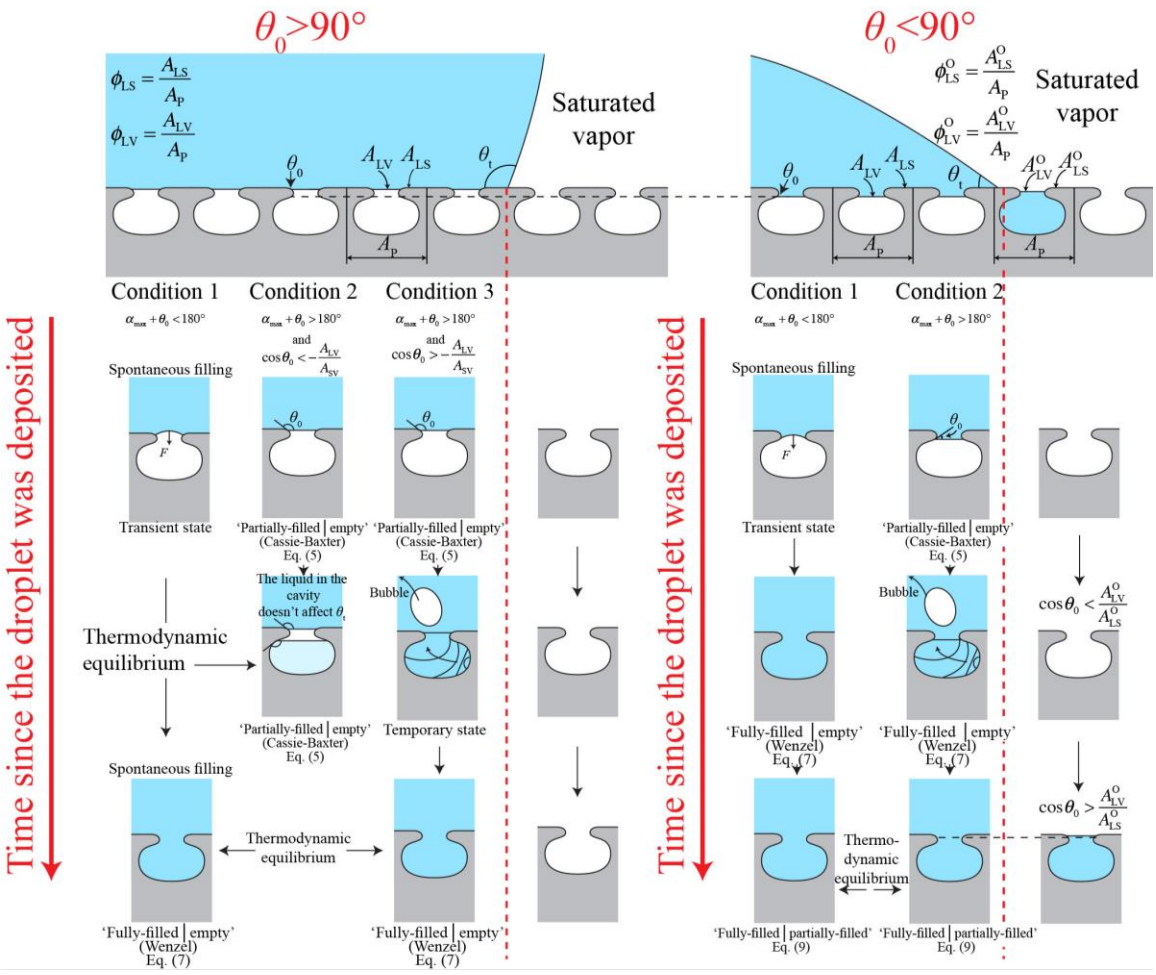

Figure S8: Schematic illustration that summarizes the different conditions that yield the three wetting states: (1) the 'partially-filled | empty' (Cassie-Baxter), (2) the 'fully-filled | empty' (Wenzel) and (3) the 'fully-filled | partially-filled' wetting state. Note that the 'partially-filled | partially-filled' is presented in this figure since it cannot be thermodynamically stable.

References

(1) Tadmor, R. Line Energy and the Relation Between Advancing, Receding, and Young Contact Angles. *Langmuir* **2004**, *20* (18), 7659–7664.

(2) Melo-Espinosa, E. A.; Sánchez-Borroto, Y.; Errasti, M.; Piloto-Rodríguez, R.; Sierens, R.; Roger-Riba, J.; Christopher-Hansen, A. Surface Tension Prediction of Vegetable Oils Using Artificial Neural Networks and Multiple Linear Regression. *Energy Procedia* **2014**, *57*, 886–895.